NACA RM E50J09

NACA

RESEARCH MEMORANDUM

EXPERIMENTAL PRESSURE DISTRIBUTIONS OVER TWO WING-BODY COMBINATIONS AT MACH NUMBER 1.9

By Barry Moskowitz and Stephen H. Maslen

Lewis Flight Propulsion Laboratory
Cleveland, Ohio

NATIONAL ADVISORY COMMITTEE
FOR AERONAUTICS

WASHINGTON
February 5, 1951

NATIONAL ADVISORY COMMITTEE FOR AERONAUTICS

RESEARCH MEMORANDUM

EXPERIMENTAL PRESSURE DISTRIBUTIONS OVER TWO WING-BODY COMBINATIONS AT MACH NUMBER 1.9

By Barry Moskowitz and Stephen H. Maslen

SUMMARY

Pressure distributions on two wing-body combinations have been obtained at a Mach number of 1.9 to investigate the wing-body interference. A rectangular wing, a triangular wing, and a cylindrical body with an ogive nose were studied alone and in combination. Both wings had a span of 14 inches, an aspect ratio of $2\frac{1}{3}$, and a 5-percent-thick double-wedge cross section. The wings were mounted on the cylindrical portion of the body. The investigation was conducted over a range of angles of attack varying in 2° increments from -4° to 4°.

The pressure distributions over the wing-body combination compared favorably with theoretical calculations based primarily on a generalization of the method of Nielsen and Matteson, except at the root section of the wings where the boundary layer of the body modified the flow.

INTRODUCTION

Although the characteristics of the flow about thin wings and about slender bodies of revolution in a supersonic stream have been extensively studied in the past few years, information concerning the effects of interference between wing and body is still needed. Theoretical studies of the problem using linearized theory are presented in references 1 to 5. In reference 6, the method of characteristics was used. Little experimental data are available, however, particularly on pressure distributions. Van Dyke (reference 7) has reported force measurements and Cramer (reference 8) has given some results that are compared with Ferrari's studies (reference 2).

In the investigation reported herein, which was conducted at the NACA Lewis laboratory, static-pressure surveys were made at a Mach number of 1.9 on two wing-body combinations; one wing was rectangular and the other triangular. The wings and the body were investigated separately for comparison. The results are compared with theoretical calculations based primarily on the method of reference 4, which was generalized to include some angle-of-attack effects.

APPARATUS AND PROCEDURE

The wing-body combinations were investigated in the NACA Lewis 18- by 18-inch supersonic wind tunnel. The Mach number, obtained from a tunnel calibration survey, was 1.90 $\pm$.01 in the vicinity of the models. The total-pressure variation along the models was $\pm$0.5 percent and was therefore neglected. The test Reynolds number, based on the mean wing chord, was 1.64×10^6.

A photograph of the models investigated is shown in figure 1 and a sketch of the models showing principle dimensions and the location of static-pressure orifices is presented in figure 2. Pressure surveys were taken at 2° increments in angle of attack from -4° to 4°. The pressures were photographically recorded from multiple-tube manometer boards using tetrabromoethane as the working fluid.

The angle of attack of the model was measured with a cathetometer during each test. Angles were accurate to $\pm.01^\circ$. Because of the low aspect ratio of the wings, aeroelastic deformation of the wing sections was considered negligible.

THEORY

The differential equation for linearized potential flow is assumed to apply. Solutions may be linearly superposed to obtain the flow over a particular configuration. The boundary condition for the flow is that the normal velocity is zero at the surface.

The wing-body problem may be solved by starting with the solution for the wing alone (reference 9 or 10) and the body alone (reference 11 or 12). When these solutions are combined, the boundary conditions are no longer satisfied because the body (at angle of attack) generates an upwash in the plane of the wing and the wing causes a flow through the body. A wing-interference potential and a body-interference potential are introduced, whose respective functions are to cancel the upwash in the plane of the wing and to cancel the flow through the body.

Consider the wing in the presence of the known body upwash field (reference 12 or 13). The required wing interference potential is readily found by the method given in reference 14, which amounts to considering a wing with a local angle of attack equal to the local upwash induced by the body divided by the free-stream velocity. In order to avoid infinite sidewash at the wing-body juncture, the upwash is taken to be continuous through the blanketed portion of the wing (region of the wing covered by the body).

The wing-interference potential plus the two basic solutions satisfy the boundary conditions on the whole wing and on the body in the region of no interaction. The remaining problem consists in canceling the flow generated through the body by the two wing potentials, without disturbing the boundary conditions on the wing. The latter condition will automatically be satisfied if the problem can be treated as symmetric with respect to the plane of the wing.

In reference 4, Nielsen and Matteson describe an approximate method to determine the body interference solution for symmetric-flow problems. The body is symmetrically divided into plane control areas with finite line pressure sources placed on each control surface normal to the free stream. The normal velocity is averaged over each area and the strengths of successive sources are determined taking into account the effect of one line source on another. Because the procedure of reference 4 gives a symmetric solution, no flow is induced across the plane of the wing.

For a symmetrical wing mounted on the body at the center line with both wing and body at zero angle of attack, the flow is symmetric. Also, those portions of an unsymmetric flow may be treated as symmetric that are not influenced by any portion of the body (in the region of interaction) lying on the opposite side of the plane of the wing. For example, in the configurations shown in the following sketch, no body-interference potential is required in region I; in region II, the body interference potential may be found by considering a symmetrical problem; and in region III the problem must be considered as unsymmetric.

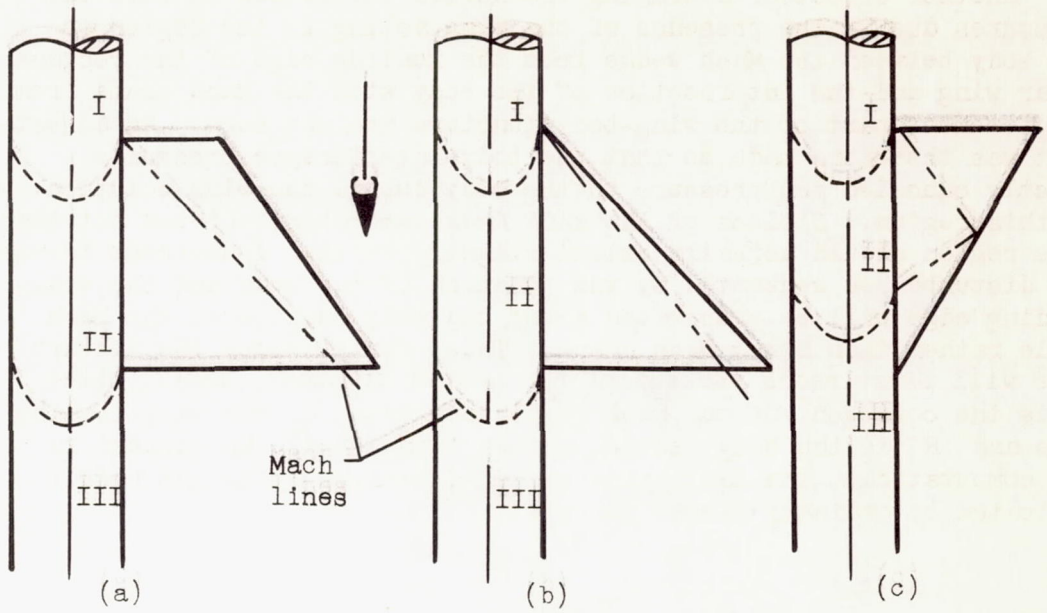

With the procedures previously discussed, the pressure distribution for a rectangular wing-body combination can be calculated in regions uninfluenced by the wing trailing edge (similar to the configuration in sketch (a)). The triangular wing investigated actually had a slightly subsonic leading edge but was assumed, for ease in computations, to have a sonic edge and is consequently similar to sketch (b). The triangular-wing solution yields infinite sidewash at the intersection of the leading edge with the body. This infinite sidewash was reduced to finite values, before calculating the body interference potential, by distribution line sources and sinks in the manner discussed in reference 4.

Superposition of the rectangular-wing solution, the wing-interference solution, and the body solution results in discontinuities in the pressure distribution on the body. The body-interference solution should therefore have corresponding discontinuities of the same magnitude but of opposite sign, inasmuch as the pressure distribution on the body should be continuous. This continuity of the pressures on the body is known from the fact that all disturbances on the body due to the wing are propagated along Mach cones, which generate no pressure discontinuities in linearized theory. The normal velocities, however, are averaged over given regions of the body; consequently, the body-interference solution fails to give these discontinuities. For this reason, the body-interference pressures were so adjusted on the body that the pressure distributions were continuous on the body.

Another effect of averaging the normal velocities is that the pressures due to the presence of the wing acting in the region on the body between the Mach wedge from the leading edge of the rectangular wing and the intersection of the body with the Mach cones from the foremost part of the wing-body juncture are not zero. An adjustment was therefore made so that the body-interference pressures exactly canceled the pressure on the body due to the wing solution in this region. Nielsen of the NACA Ames laboratory pointed out that this region should actually extend slightly farther downstream because the disturbances generated by the junction of the body and the wing leading edge will be propagated along the body surface at the Mach angle rather than along Mach cones. Thus, for example, the disturbance will first reach the top of the body a distance $\beta R\pi/2$, where β is the cotangent of the Mach angle downstream of the wing leading edge and R is the body radius, rather than $\beta R\sqrt{2}$ as assumed in the computation. The last value was used because it is the result indicated by ordinary linear theory.

RESULTS

Experimental data are presented and compared with theoretical results in figures 3 to 13. The pressure coefficient C_p and the change in pressure with angle of attack $dC_p/d\alpha$, both evaluated at $\alpha = 0$, are plotted for each orifice location. Within the limited range of angles of attack of the investigation, the faired variation of C_p with angle of attack was approximately linear. The experimental results for the body alone, rectangular wing alone, and triangular wing alone are given in figures 3, 4, and 5, respectively. In figure 3 the experimental value of $\frac{dC_p/d\alpha}{\sin\theta}$, where θ is the angle measured around the body from the plane of the wing, is obtained by averaging the various values of $\frac{dC_p/d\alpha}{\sin\theta}$. The agreement between theory and experiment in figures 3, 4, and 5 is the basis for determining the accuracy of the interference calculation. For example, if the difference between experiment and theory for a component in combination is within the order of agreement existing between theory and experiment for the component alone, the agreement is considered good.

Rectangular Wing and Body

Results for the rectangular wing in the presence of the body are presented in figure 6. Because of the large nose angle of the body

(30° half angle), a fairly strong shock was generated (fig. 14). In the neighborhood of the wing tip, the shock wave occurred approximately 2 inches upstream of the Mach wave assumed by linear theory. As a result the pressures predicted by linear theory, in the forward part of the tip region, are higher than the experimental values. As shown in the schlieren photograph, the nose shock reflects off the tunnel walls and intersects the wing tip. Because of the increase in pressure across the reflected shock, the experimental values are higher than those obtained by linear theory in the rearward portion of the tip region. In the plane of wing, however, the body does not directly cause any change in pressure due to angle of attack. Moreover, the shock position does not vary appreciably over the range of angles of attack of the investigation. The effects of the shock and its reflection therefore cause no discrepancy between the theoretical and experimental values of $dC_p/d\alpha$ on the wing.

At the root section, the boundary layer of the body modified the flow over the wing. In particular, the discontinuity in the slope of the wing was softened, thereby decreasing the pressure change predicted by linear theory. At the wing midspan position, none of these difficulties occurred and close agreement between linear theory and experiment was obtained.

In order to illustrate the effect of the presence of the body on the pressures acting on the rectangular wing, the increments ΔC_p and $\Delta\frac{dC_p}{d\alpha}$ due to the presence of the body are presented in figure 7. The theoretical curves and the experimental points were obtained by taking the difference between corresponding values in figures 6 and 4. For zero angle of attack, the section wave drag of the wing in combination is less than the corresponding section wave drag of the wing alone, if the increment in pressure is negative over the positively sloped portion of the wing and positive over the negatively sloped portion. In the root section the experimental points, but not the theoretical curve, indicate less section drag. In the midspan region the experimental points indicate slightly less section drag, whereas the section drag indicated by the theoretical curve remains about the same. In the tip region, both theoretical and experimental values indicate an increase in the section drag, which is to be expected inasmuch as the tip region of the rectangular wing is influenced by the pressure gradient associated with the nose of the body. Because of a large reduction in the drag of the wing due to the blanketing of the center section, the over-all wave drag of the combination is probably less than the sum of the wave drags of the components.

Inasmuch as the increment in $dC_p/d\alpha$ is negative on the top surface of the wing, the sectional lift is greater than the corresponding sectional lift of the wing alone. This result is to be expected because the presence of the body at angle of attack causes an upwash field, which increases the effective wing angle of attack. (See the section THEORY.)

The experimental variation of C_p and $dC_p/d\alpha$ on the body in the presence of the rectangular wing is presented in figures 8(a) and 8(b), respectively. Close agreement was obtained for the slope of the pressure coefficient curve. For zero angle of attack, the trend of the experimental points and the theoretical curves appear to be similar. The quantitative agreement is of the order obtained for the wings and the body alone.

The increments in C_p and $dC_p/d\alpha$ on the body due to the presence of the wing are presented in figures 9(a) and 9(b), respectively. In figure 9(a) the direct influence of the wing is noted in the increases and decreases in body pressure coefficient in the regions influenced by the positive and negative wing slopes, respectively. Because the $\Delta\frac{dC_p}{d\alpha}$ curve in figure 9(b) is negative, an increase in lift results on the body due to the presence of the wing.

Triangular Wing and Body

The experimental results for the triangular wing in the presence of the body are shown in figure 10. Reasonably good agreement with linear theory was obtained at all stations except for the root section at $\alpha = 0$, where, as was noted in the case of the rectangular wing, the theoretical discontinuity in pressure is modified by the boundary layer of the body. Inasmuch as the body nose shock was not near the triangular wing at any point, the poor correlation between theory and experiment noted in the outboard region of the rectangular wing does not occur for this case.

The increments ΔC_p and $\Delta\frac{dC_p}{d\alpha}$ on the triangular wing due to the presence of the body are presented in figure 11. At the outboard section A, the experimental points and the theoretical curve for $\alpha = 0$ indicate a slight decrease in section drag relative to the drag of the wing alone. At the midspan section B, the experimental points indicate a slight decrease in section drag, whereas the theoretical

curve indicates that the section drag remains about the same for $\alpha = 0$. Both the experimental points and the theory at the inboard section C show a sizeable decrease in section drag over that for the triangular wing alone at $\alpha = 0$. Thus at zero angle of attack, the over-all wave drag of the triangular wing-body combination is less than the sum of the wave drags of the components. At sections A and B, the fact that the experimental points of $\Delta dC_p/d\alpha$ are negative indicates a slight increase in section lift, although the theoretical curves at these stations indicate that the section lift remains unchanged. At the root section C, both linear theory and experiment show a decrease in section lift.

Experimental results for C_p and $dC_p/d\alpha$ on the body in the presence of the triangular wing are presented in figures 12(a) and 12(b), respectively. The difference between experiment and linear theory in figure 12(a) is very nearly that displayed by the curves for the body alone (fig. 3), which indicated that the interference was accurately predicted by the theory. This agreement is also shown in figures 13(a) and 13(b), where the differences in C_p and $dC_p/d\alpha$ for the body in combination with the triangular wing and the body alone are presented.

CONCLUDING REMARKS

Experimental pressure distributions at a Mach number of 1.9 were obtained for a rectangular wing and a triangular wing in combination with an ogive-nose body.

The procedure of Nielsen and Matteson was applied at zero angle of attack and a generalization of this method was used to calculate interference effects at angle of attack. The experimental results compared favorably with these theoretical calculations, except at the root section of the wings, where the boundary layer of the body modified the flow over the slope discontinuity of the wing and thereby decreased the pressure change predicted by linear theory.

Lewis Flight Propulsion Laboratory,
National Advisory Committee for Aeronautics,
Cleveland, Ohio.

REFERENCES

1. Lagerstrom, P. A., and Van Dyke, M. D.: General Considerations about Planar and Non-Planar Lifting Systems. Rep. No. SM-13432, Douglas Aircraft Co., Inc., June 1949.

2. Ferrari, Carlo: Interference between Wing and Body at Supersonic Speeds - Theory and Numerical Application. Jour. Aero. Sci., vol. 15, no. 6, June 1948, pp. 317-336.

3. Spreiter, John R.: The Aerodynamic Forces on Slender Plane- and Cruciform-Wing and Body Combinations. NACA Rep. 962, 1950. (Formerly NACA TNs 1897 and 1662.)

4. Nielsen, Jack N., and Matteson, Frederick H.: Calculative Method for Estimating the Interference Pressure Field at Zero Lift on a Symmetrical Swept-Back Wing Mounted on a Circular Cylindrical Body. NACA RM A9E19, 1949.

5. Browne, S. H., Friedman, L., and Hodes, I.: A Wing-Body Problem in a Supersonic Conical Flow. Jour. Aero. Sci., vol. 15, no. 8, Aug. 1948, pp. 443-452.

6. Ferrari, Carlo: Interference between Wing and Body at Supersonic Speeds - Analysis by the Method of Characteristics. Jour. Aero. Sci., vol. 16, no. 7, July 1949, pp. 411-437.

7. Van Dyke, Milton D.: Aerodynamic Charcteristics Including Scale Effect of Several Wings and Bodies Alone and in Combination at a Mach Number of 1.53. NACA RM A6K22, 1946.

8. Cramer, R. H.: Some Theoretical and Experimental Results for Wing-Body Interference at Supersonic Velocities. Bull. Bumblebee Aero. Symposum (Johns Hopkins Univ.), Nov. 4-5, 1948, pp. 267-276.

9. Evvard, John C.: Use of Source Distributions for Evaluating Theoretical Aerodynamics of Thin Finite Wings at Supersonic Speeds. NACA Rep. 951, 1950.

10. Lagerstrom, P. A.: Linearized Supersonic Theory of Conical Wings - (Corrected Copy). NACA TN 1685, 1950.

11. von Kármán, Theodor, and Moore, Norton B.: Resistance of Slender Bodies Moving with Supersonic Velocities, with Special Reference to Projectiles. Trans. A.S.M.E., vol. 54, no. 23, Dec. 15, 1932, pp. 303-310.

12. Tsien, Hsue-Shen: Supersonic Flow over an Inclined Body of Revolution. Jour. Aero. Sci., vol. 5, no. 12, Oct. 1938, pp. 480-483.

13. Beskin, Leon: Determination of Upwash around a Body of Revolution at Supersonic Velocities. DEVF Memo. BB-6, Consolidated Vultee Aircraft Corp., May 27, 1946.

14. Mirels, Harold: Theoretical Method for Solution of Aerodynamic Forces on Thin Wings in Nonuniform Supersonic Stream with an Application to Tail Surfaces. NACA TN 1736, 1948.

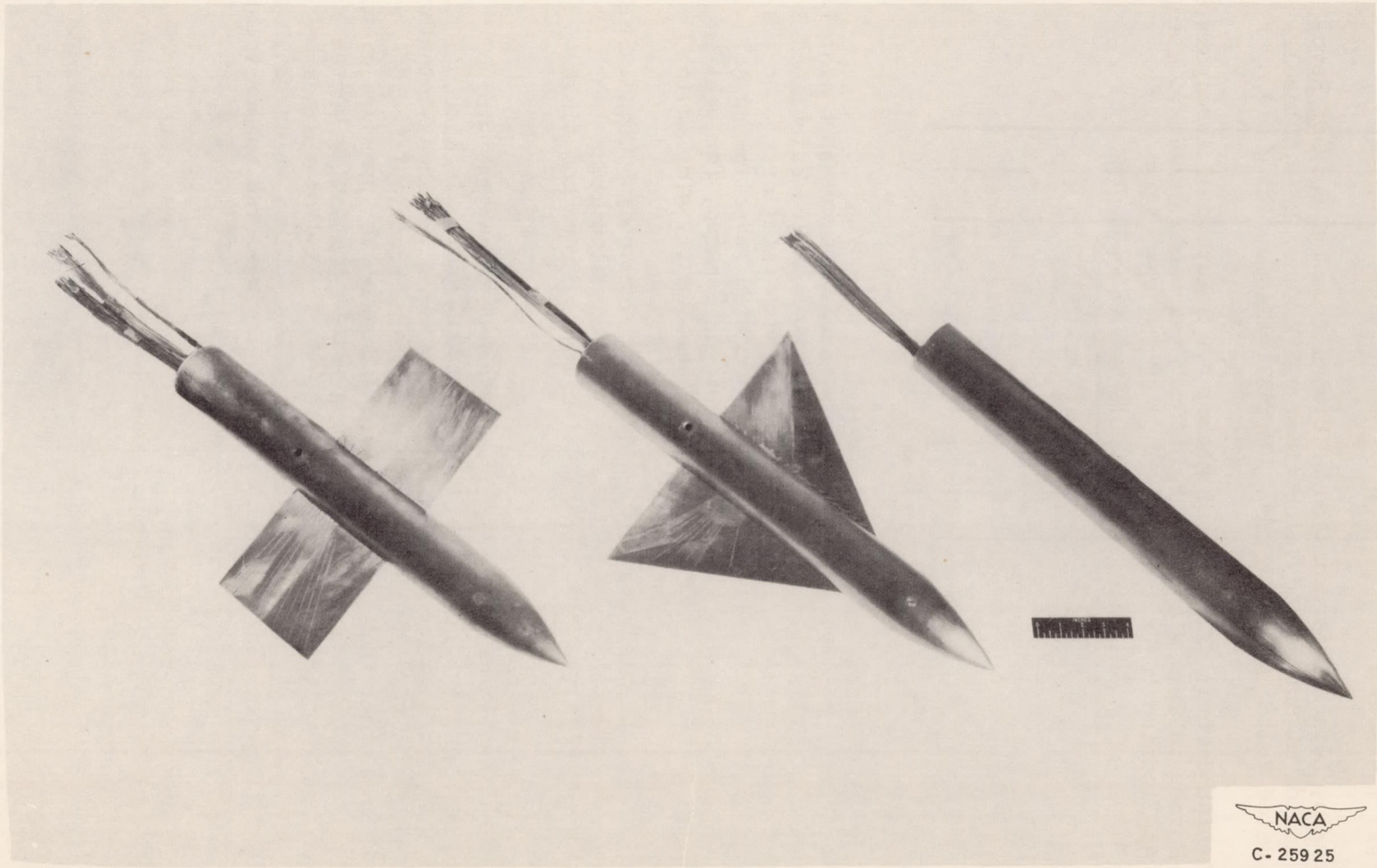

Figure 1. - Rectangular and triangular wings with ogive-nose body.

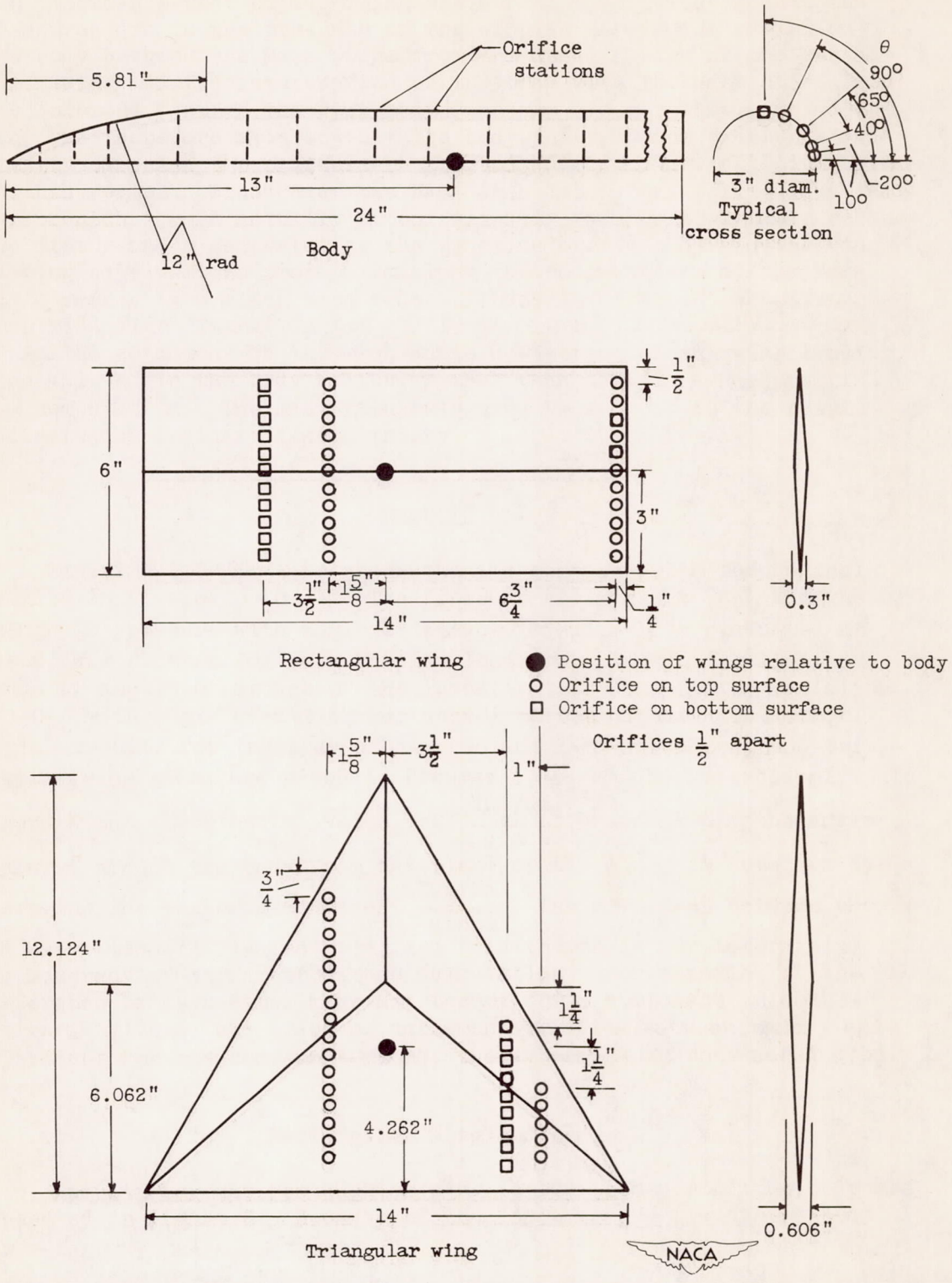

Figure 2. - Dimensioned sketch of models showing pressure orifices.

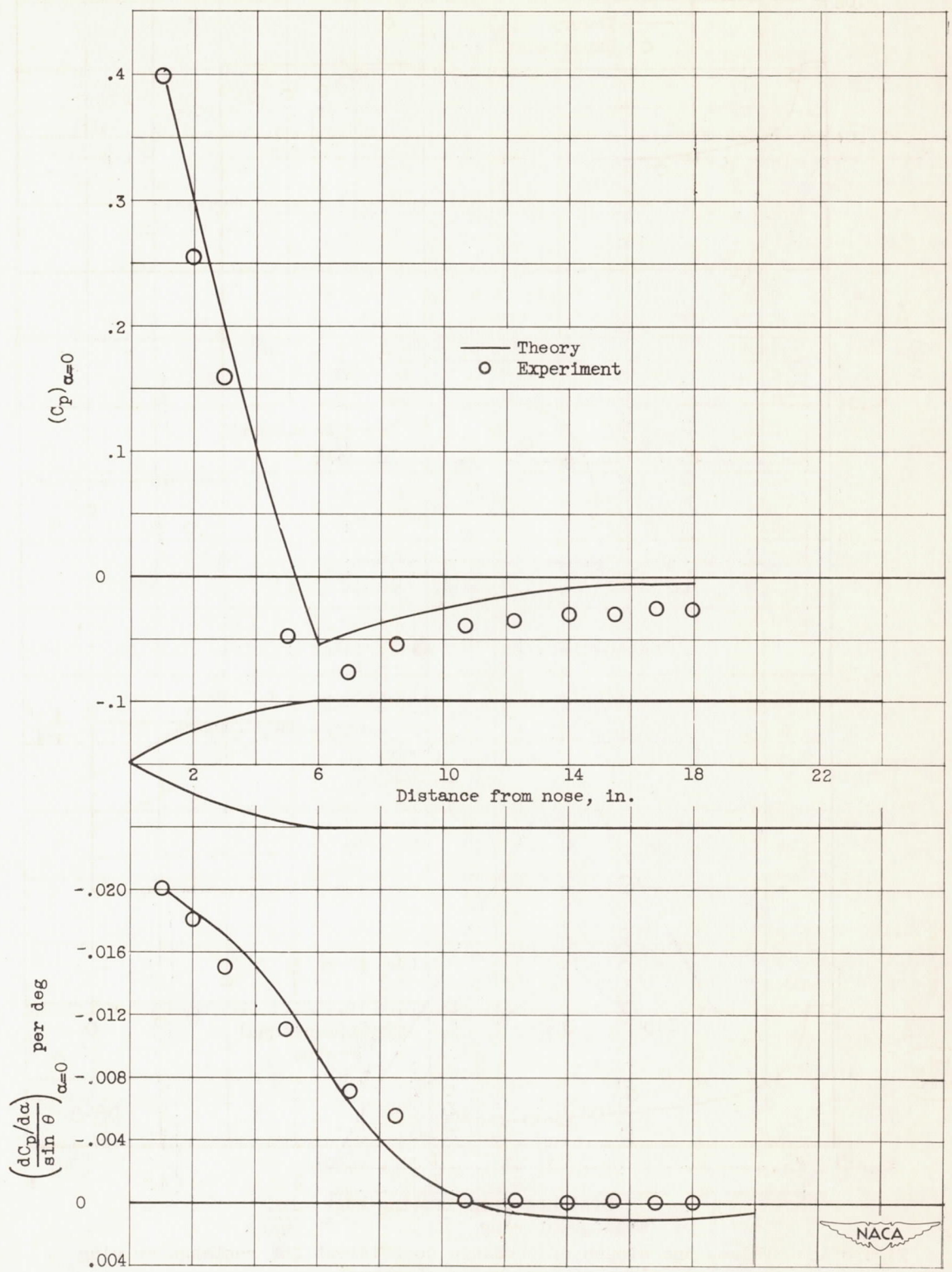

Figure 3. - Values and slopes of pressure coefficient for body alone at zero angle of attack.

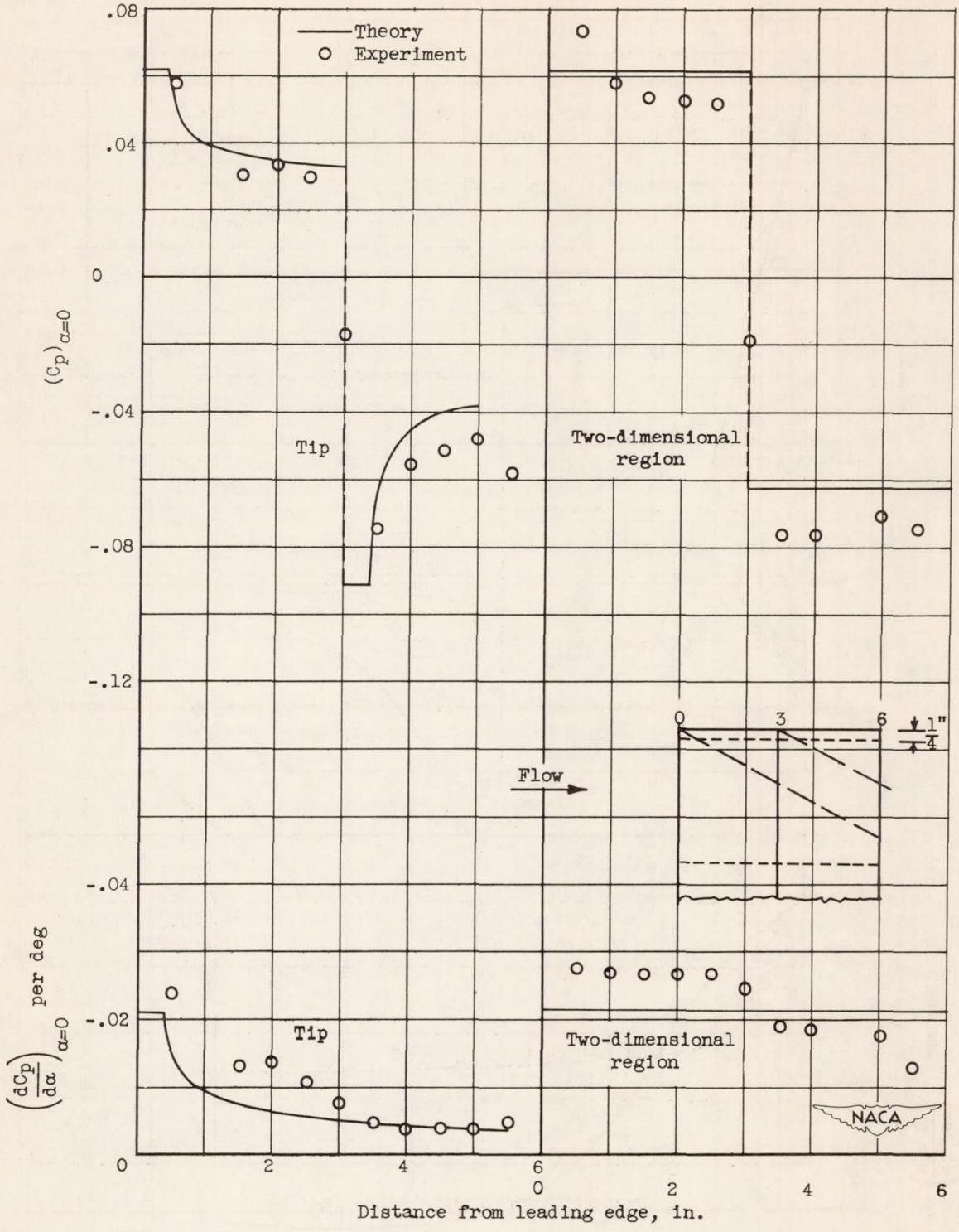

Figure 4. - Values and slopes of pressure coefficient for rectangular wing alone at zero angle of attack.

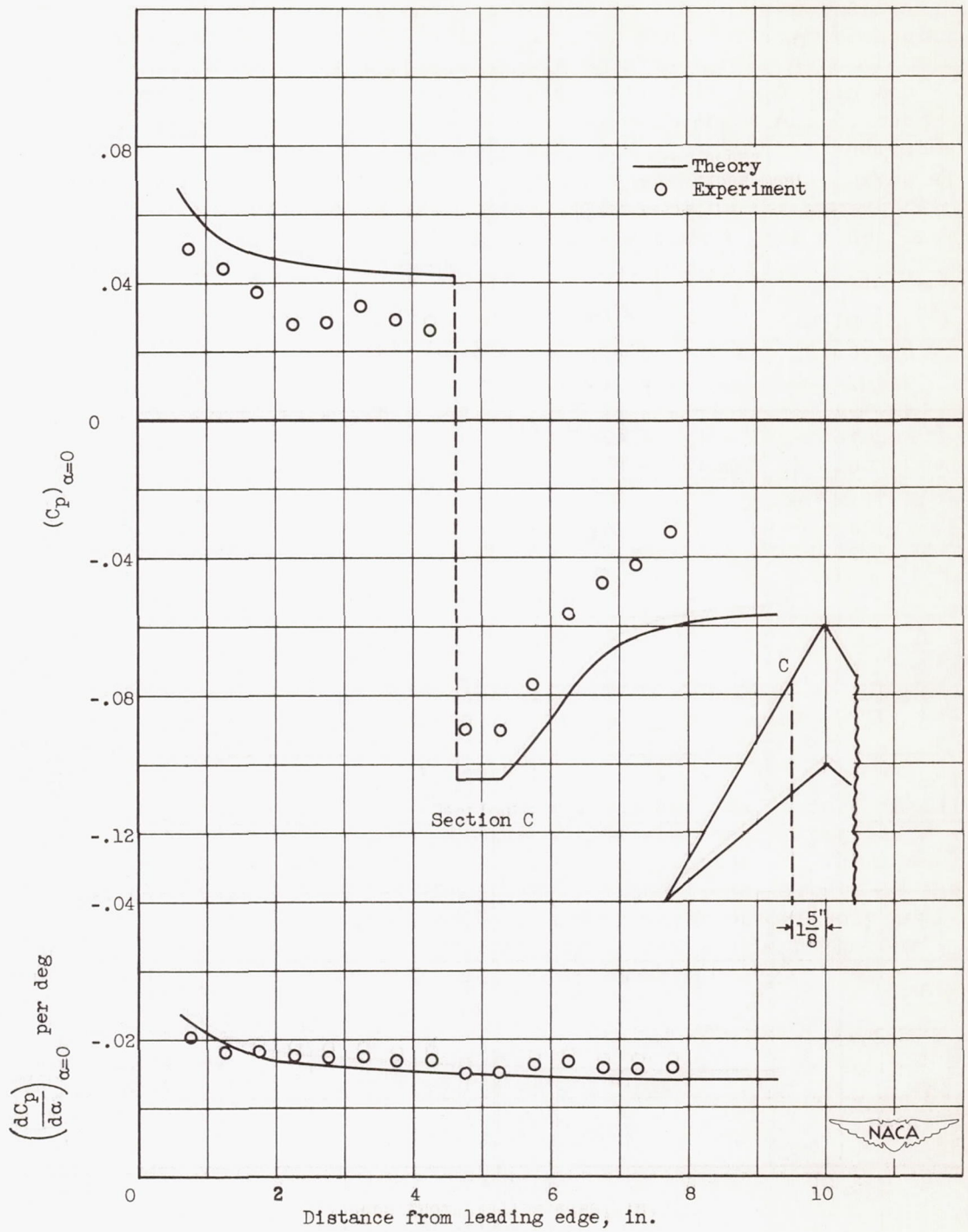

(a) Inboard station.

Figure 5. - Values and slopes of pressure coefficient for triangular wing alone at zero angle of attack.

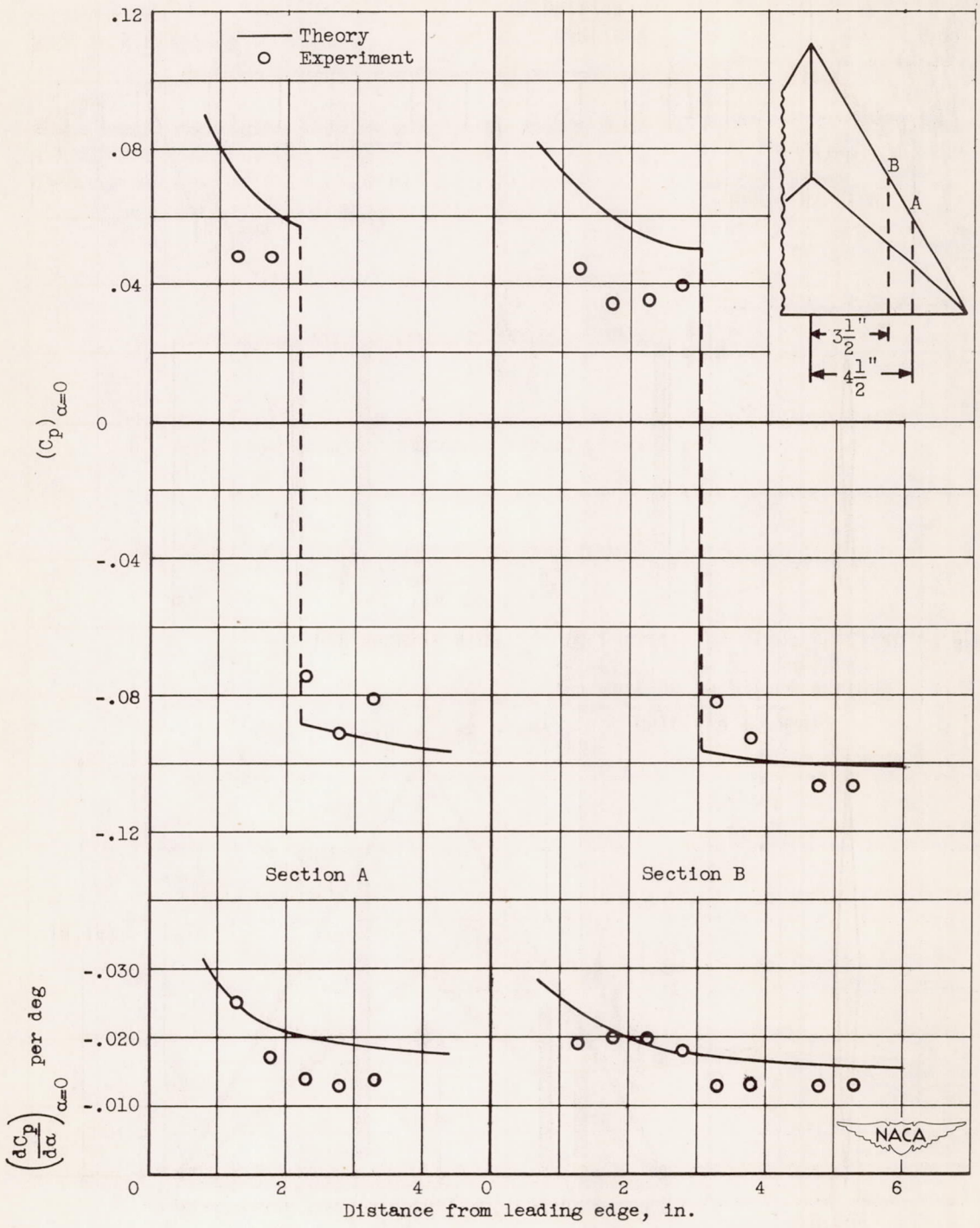

(b) Outboard stations.

Figure 5. - Concluded. Values and slopes of pressure coefficient for triangular wing alone at zero angle of attack.

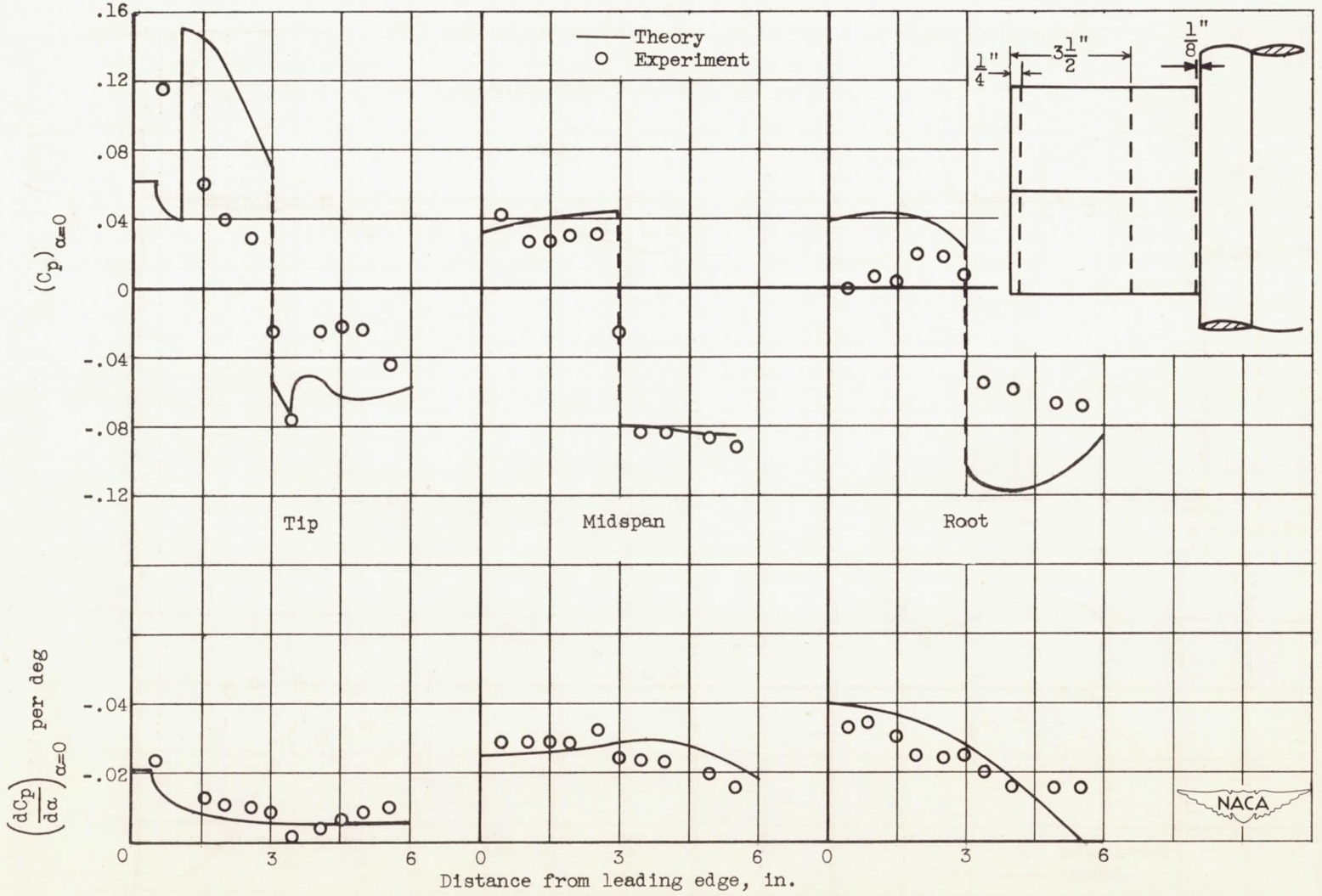

Figure 6. - Values and slopes of pressure coefficient for rectangular wing in presence of body at zero angle of attack.

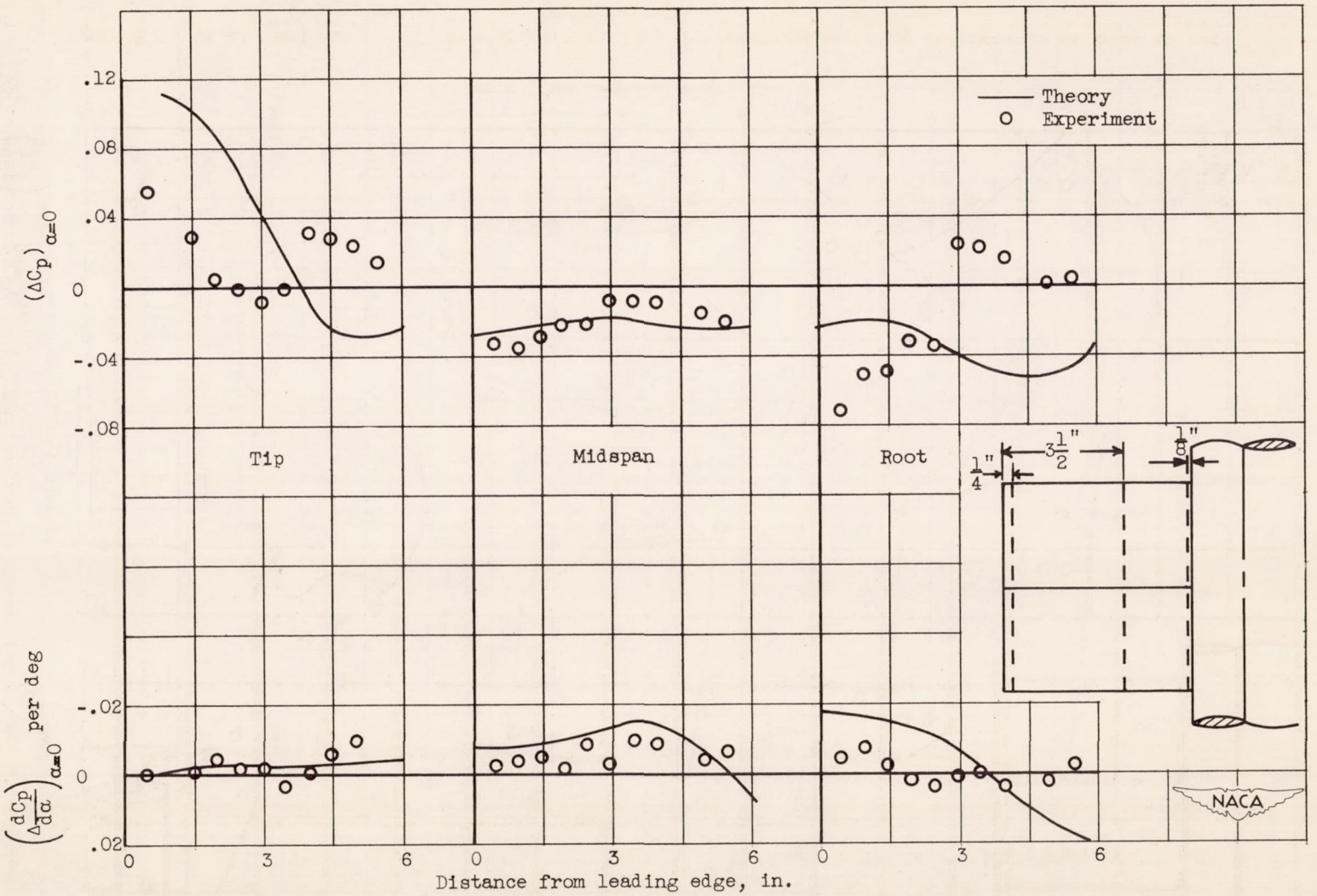

Figure 7. - Incremental values and slopes of pressure coefficient for rectangular wing due to presence of body at zero angle of attack.

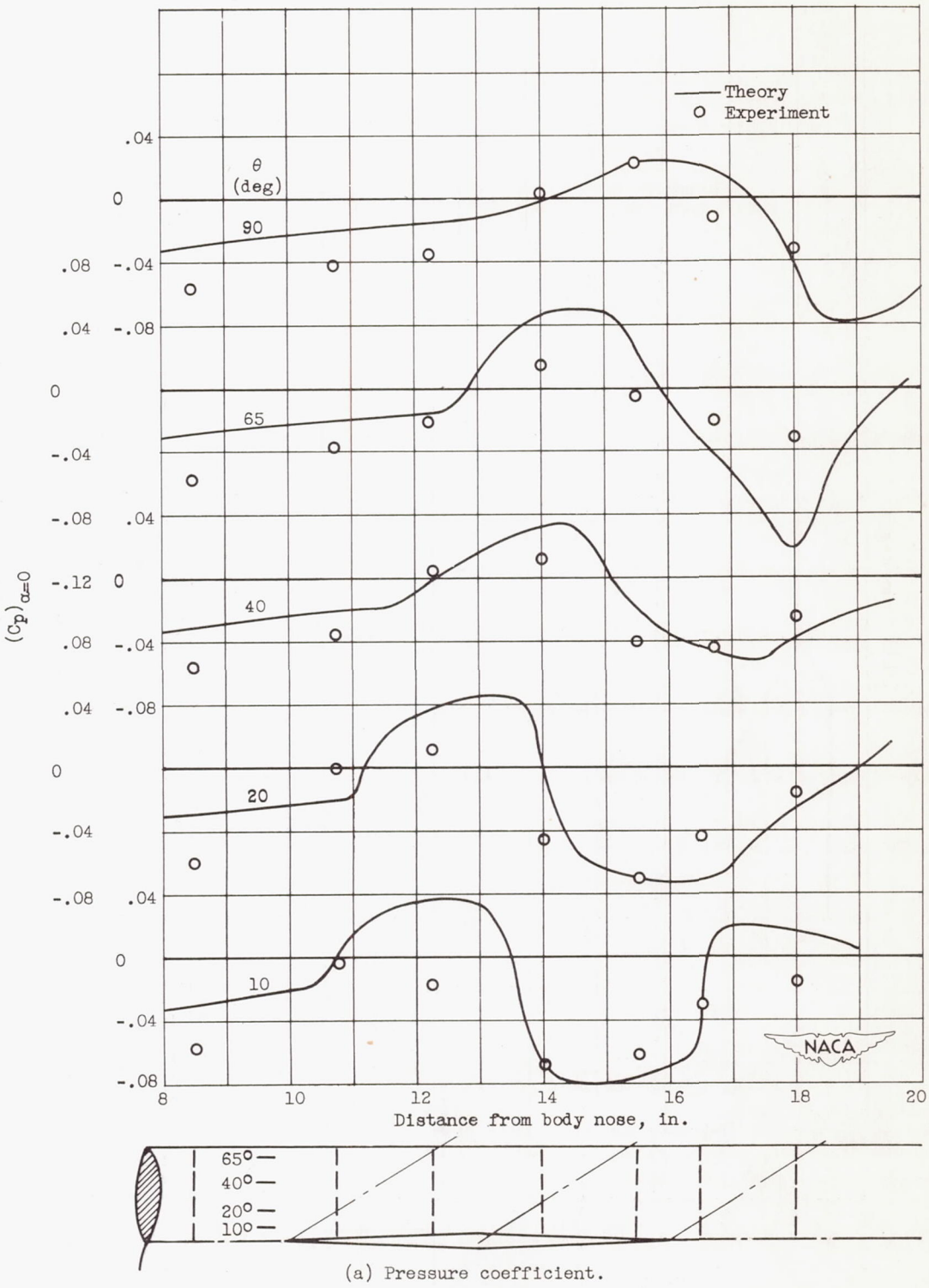

(a) Pressure coefficient.

Figure 8. - Values and slopes of pressure coefficient on body in presence of rectangular wing at zero angle of attack.

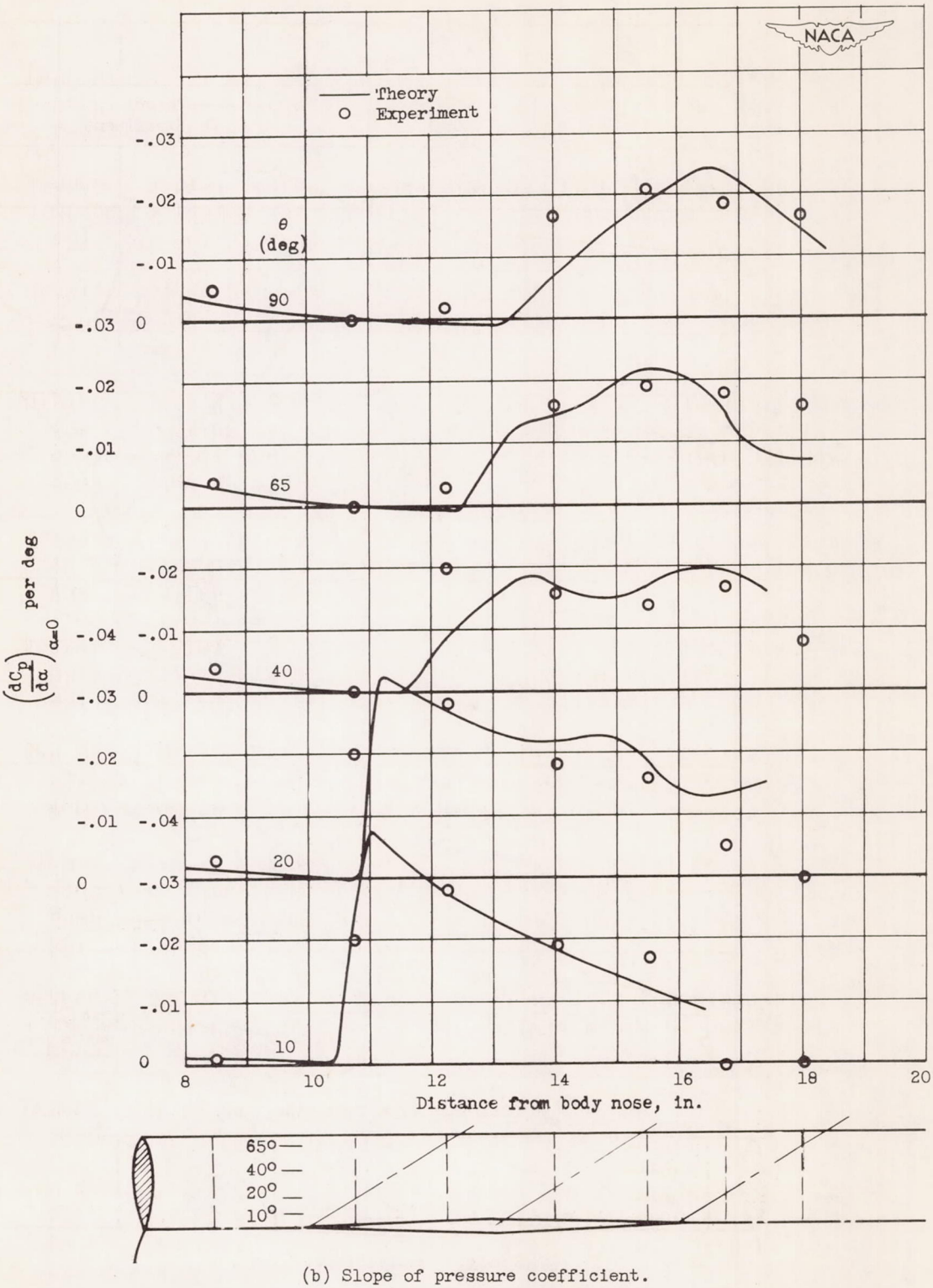

(b) Slope of pressure coefficient.

Figure 8. - Concluded. Values and slopes of pressure coefficient on body in presence of rectangular wing at zero angle of attack.

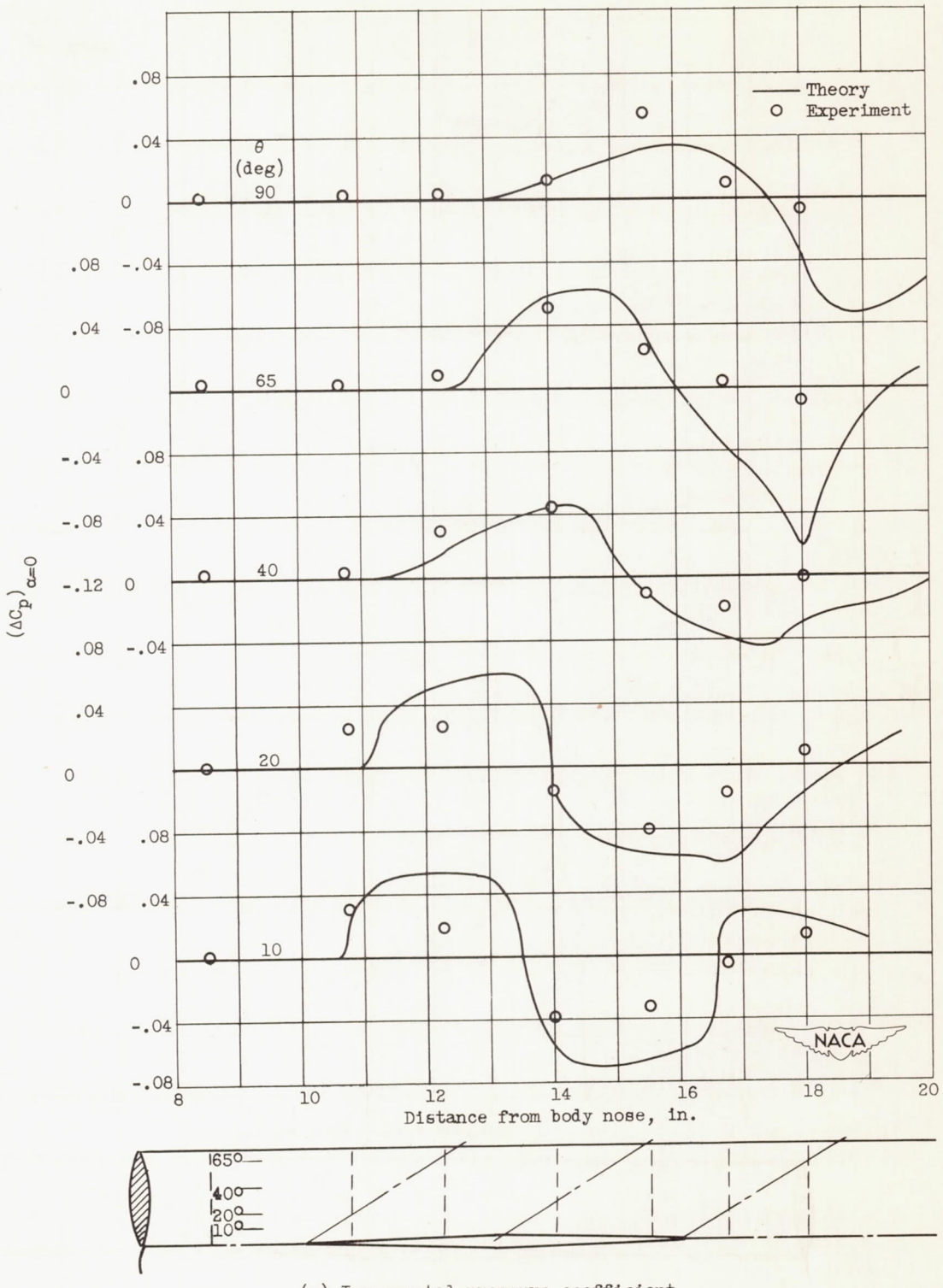

(a) Incremental pressure coefficient.

Figure 9. - Incremental values and slopes of pressure coefficient on body due to presence of rectangular wing at zero angle of attack.

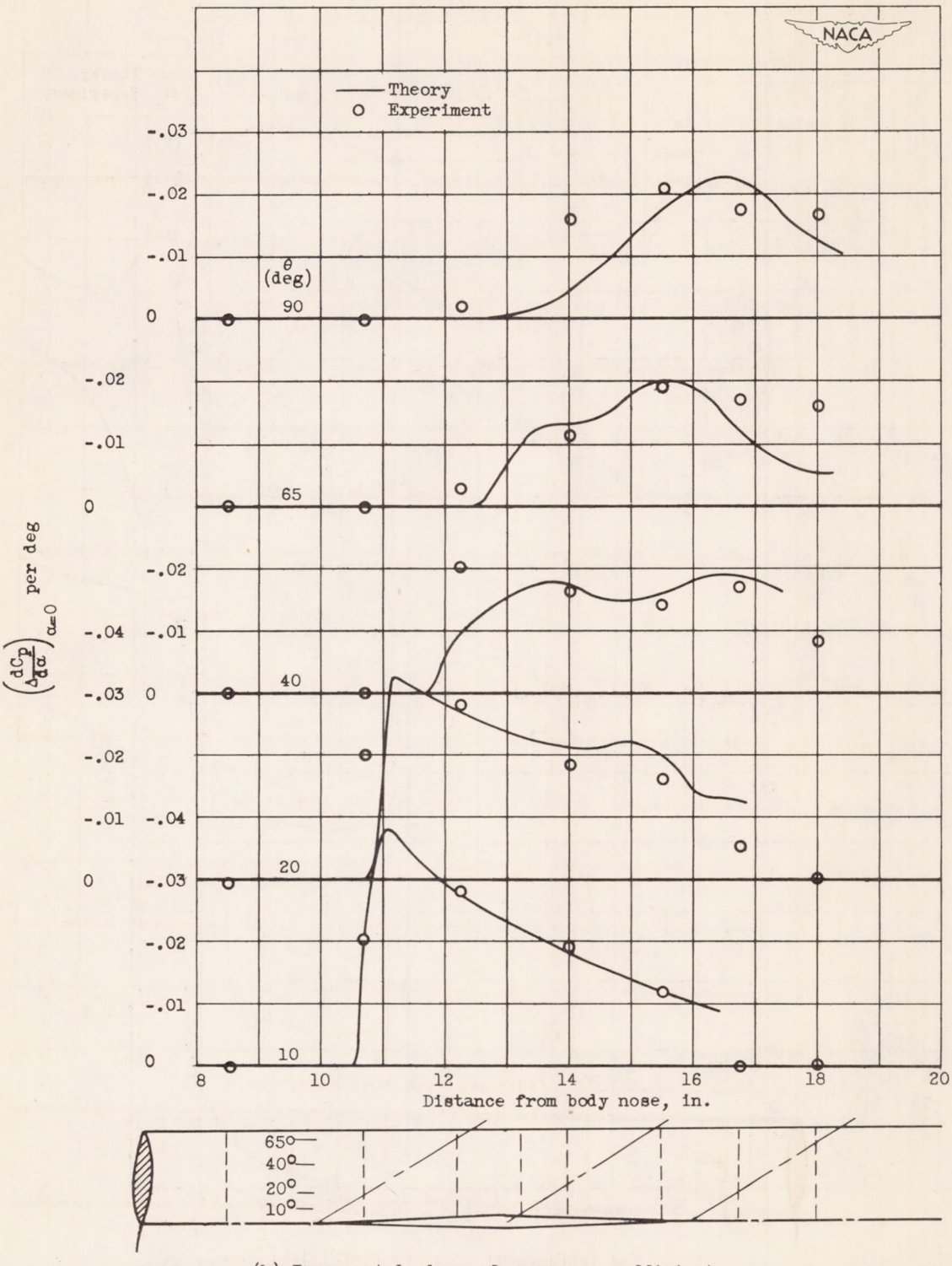

(b) Incremental slope of pressure coefficient.

Figure 9. - Concluded. Incremental values and slopes of pressure coefficient on body due to presence of rectangular wing at zero angle of attack.

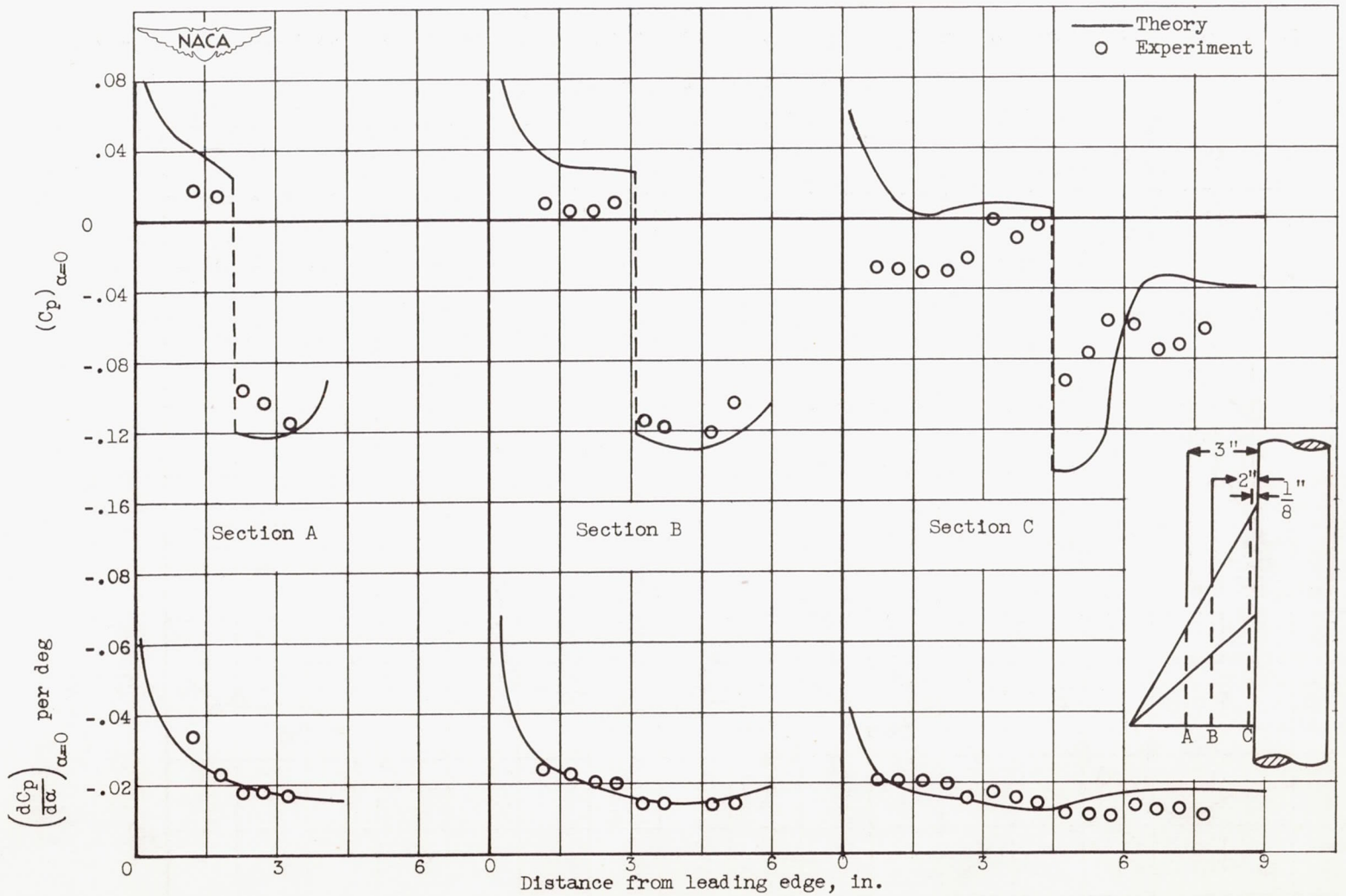

Figure 10. - Values and slopes of pressure coefficient for triangular wing in presence of body at zero angle of attack.

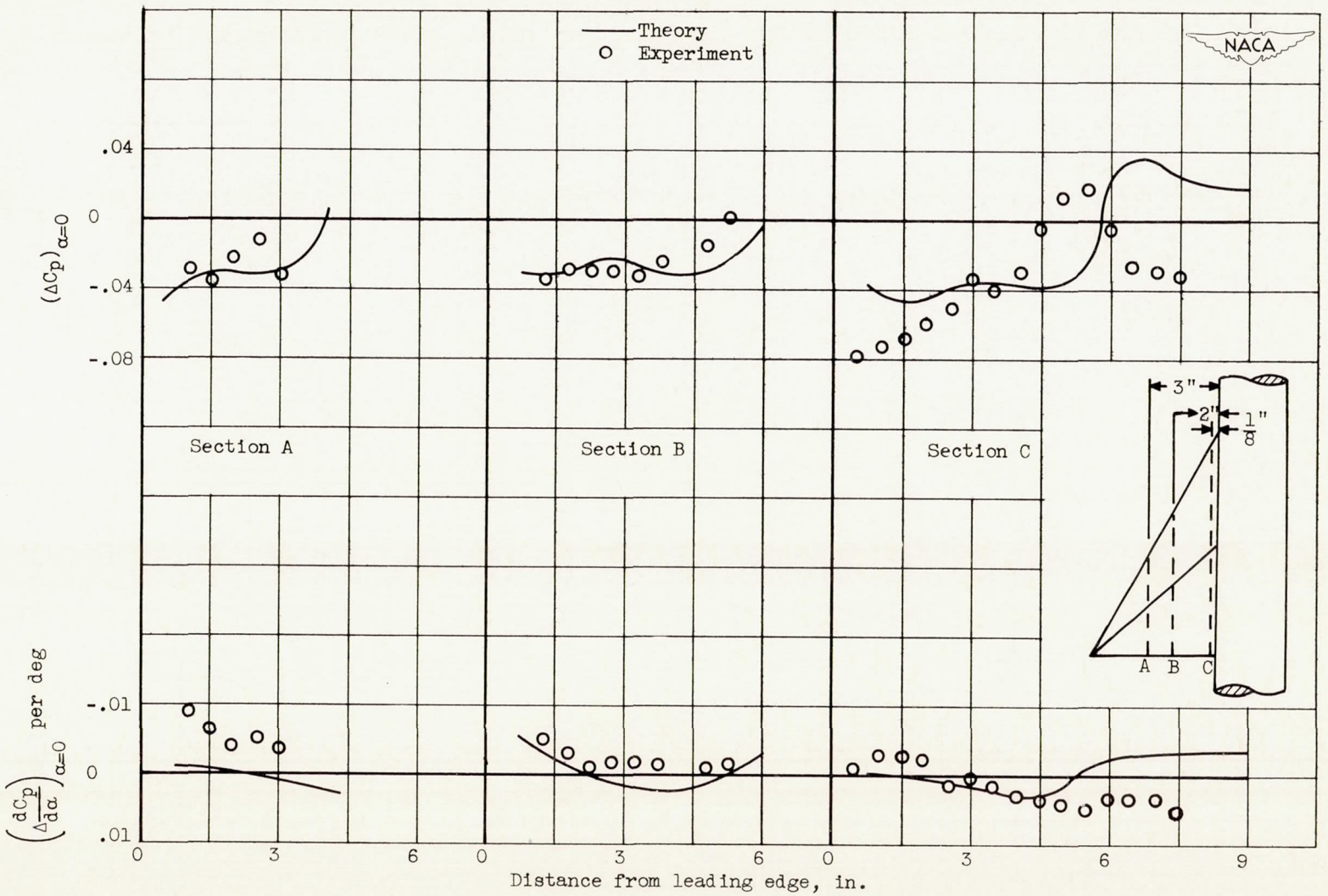

Figure 11. - Incremental values and slopes of pressure coefficient for triangular wing due to presence of body at zero angle of attack.

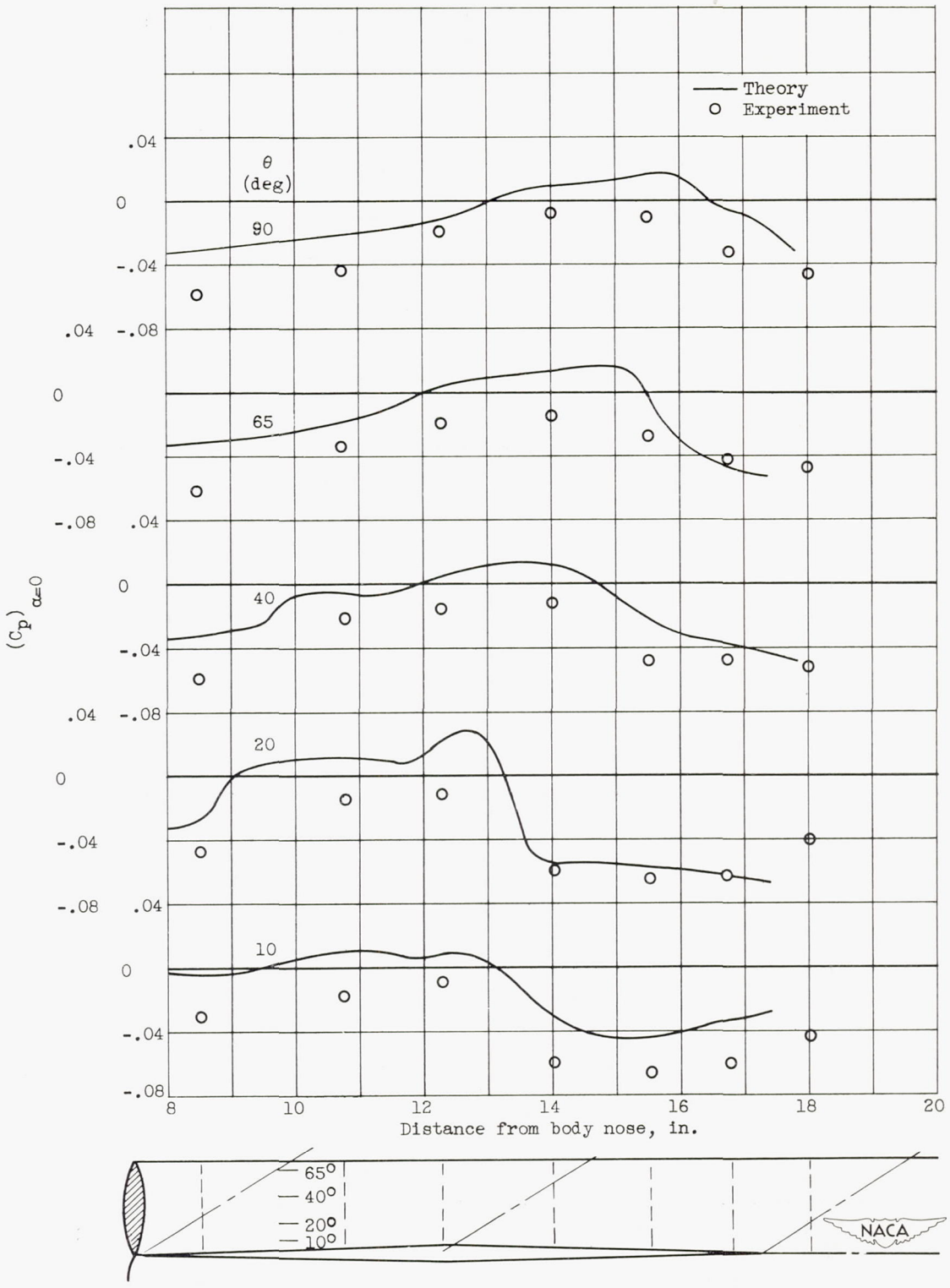

(a) Pressure coefficient.

Figure 12. - Values and slopes of pressure coefficient on body in presence of triangular wing at zero angle of attack.

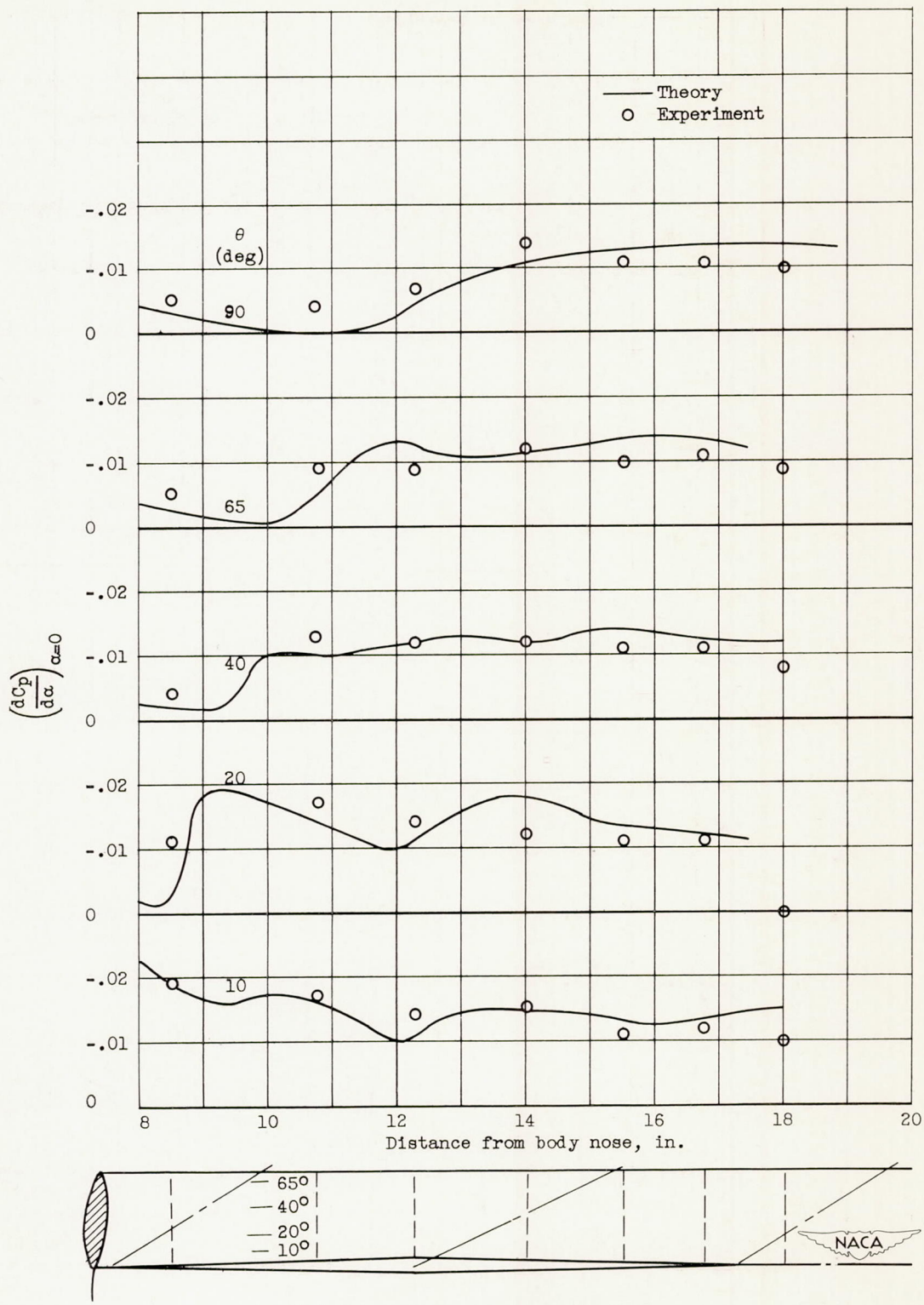

(b) Slope of pressure coefficient.

Figure 12. - Concluded. Values and slopes of pressure coefficient on body in presence of triangular wing at zero angle of attack.

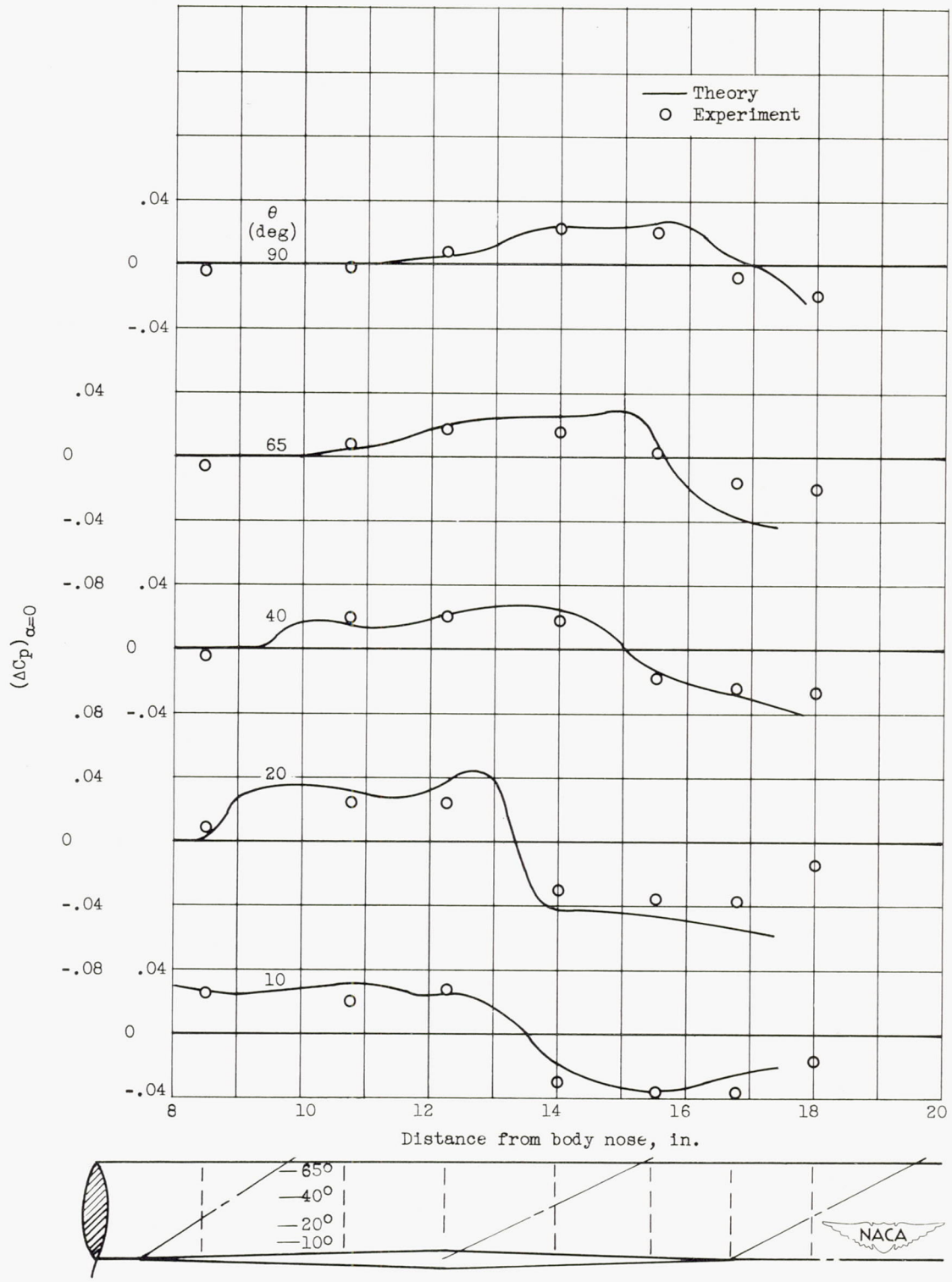

(a) Incremental pressure coefficient.

Figure 13. - Incremental values and slopes of pressure coefficient on body due to presence of triangular wing at zero angle of attack.

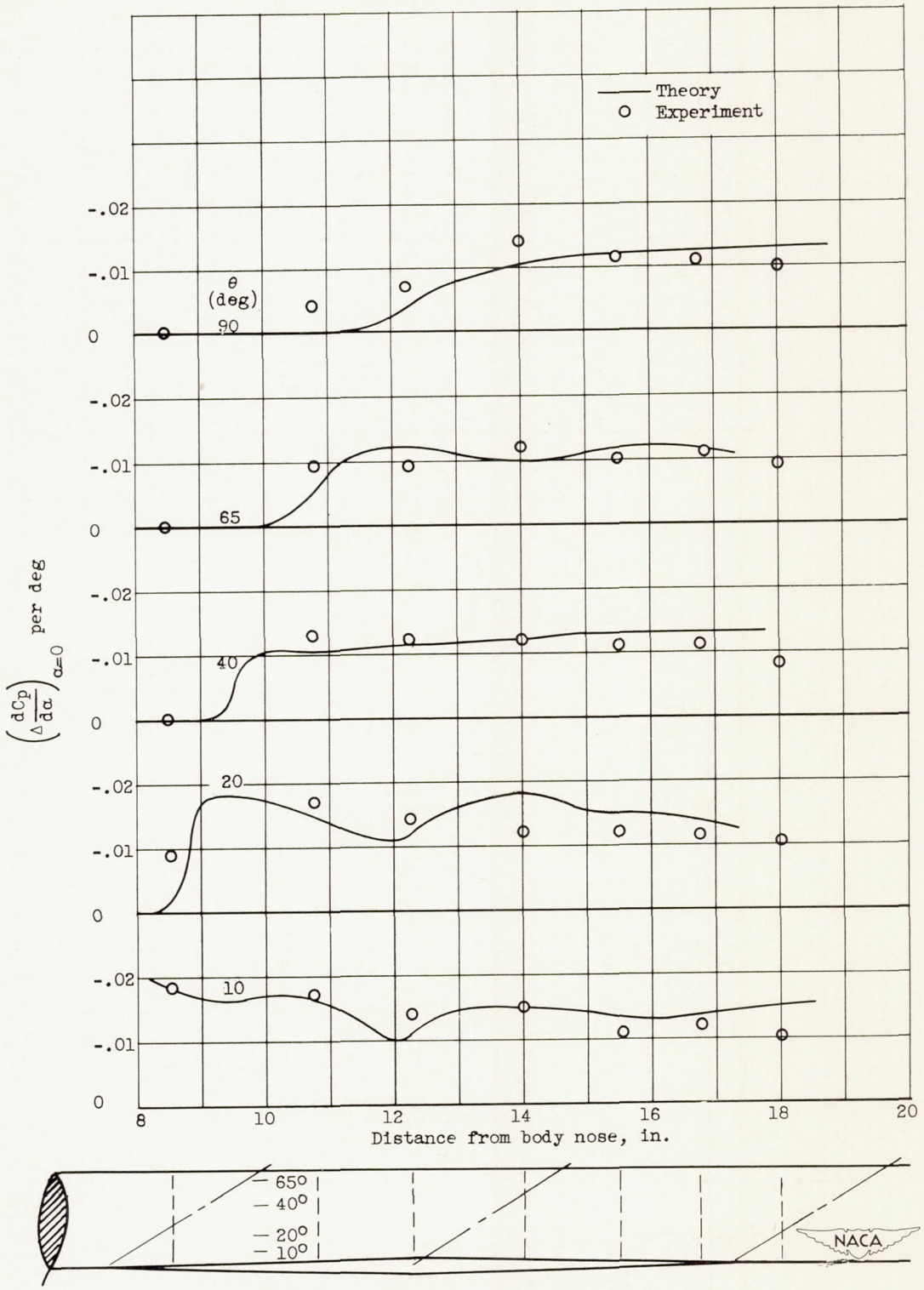

(b) Incremental slope of pressure coefficient.

Figure 13. - Concluded. Incremental values and slopes of pressure coefficient on body due to presence of triangular wing at zero angle of attack.

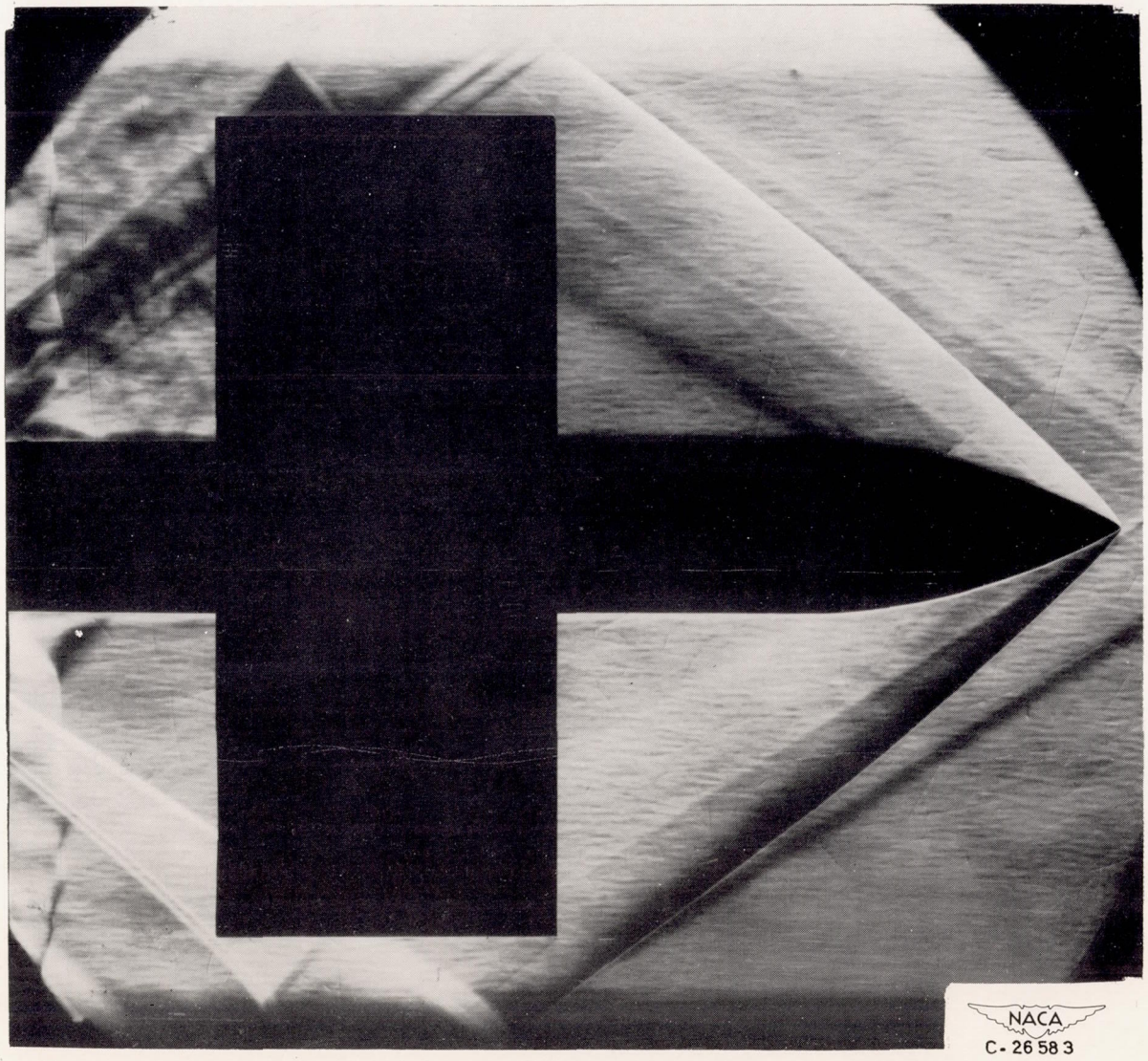

Figure 14. - Schlieren photograph of flow about rectangular wing-body combination.